Supporting Information: Mixed-Matrix Membranes Formed from Imide-Functionalized UiO-66-NH_2 for Improved Interfacial Compatibility

*Qihui Qian, Albert X. Wu, Won Seok Chi, Patrick A. Asinger, Sharon Lin, Asia Hypsher and Zachary P. Smith**

* Email address: zpsmith@mit.edu

Department of Chemical Engineering, Massachusetts Institute of Technology, Cambridge, MA 02139, United States

Section A: Supporting characterization results for the Pure MOF and PSM-MOF

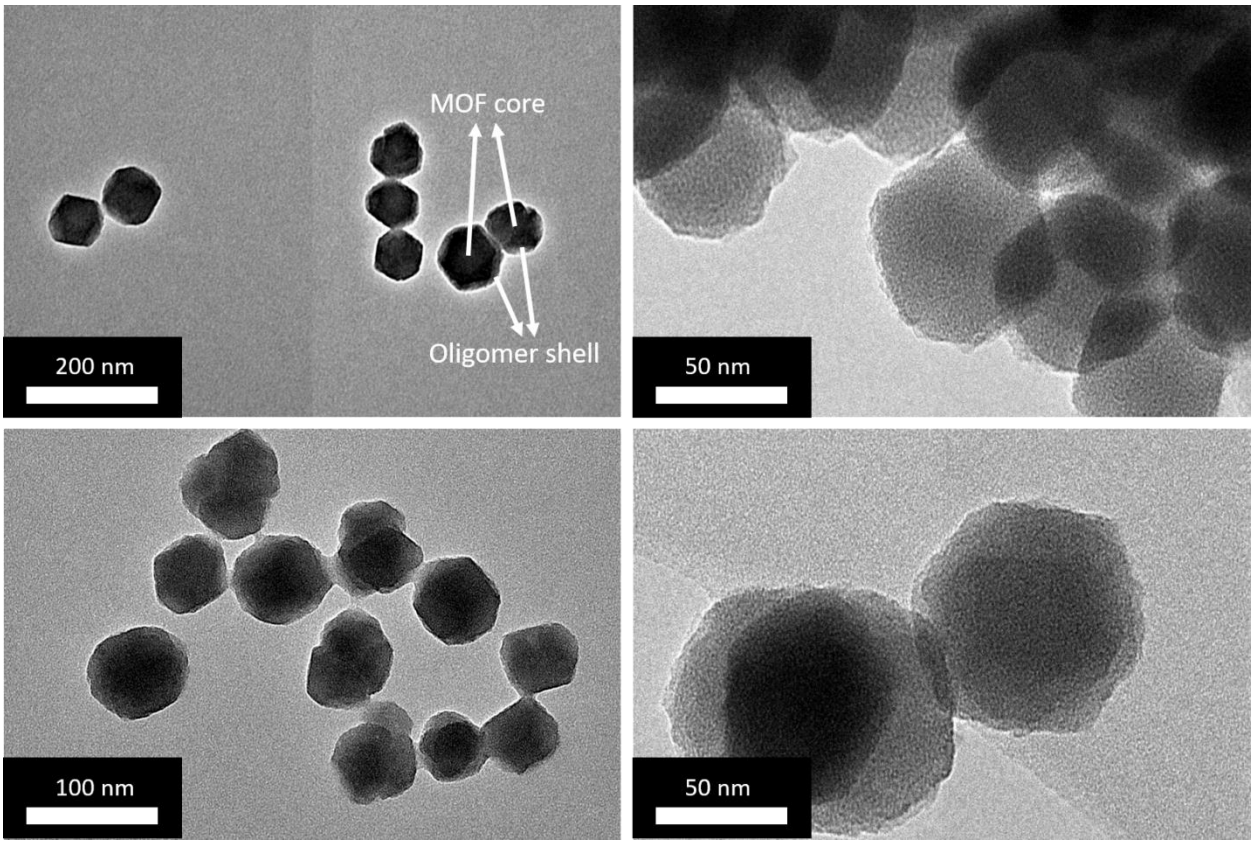

Figure S1. TEM images of oligomer-coated UiO-66-NH_2 under different magnifications. MOF core and oligomer shell are labeled in the left top image. Different surface structures can be observed between these PSM-MOF structures and the pure-MOF structures, as shown in Figure 2.

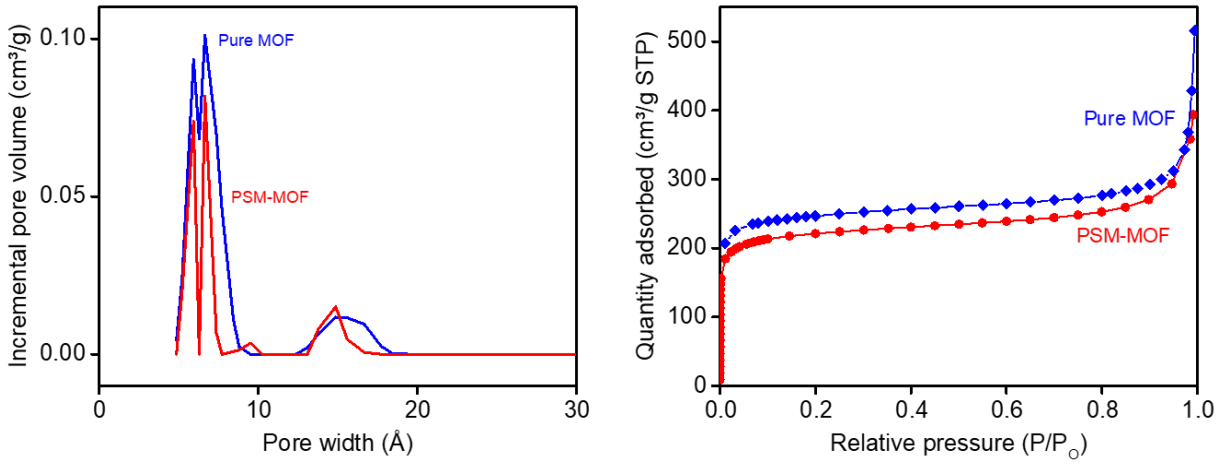

Figure S2. Pore size distribution and N_2 adsorption isotherms for Pure MOF and PSM-MOF. Pore size distribution was calculated using the built-in function of Micromeritics 3Flex Share software based on N_2@Tarazona NLDFT Model.

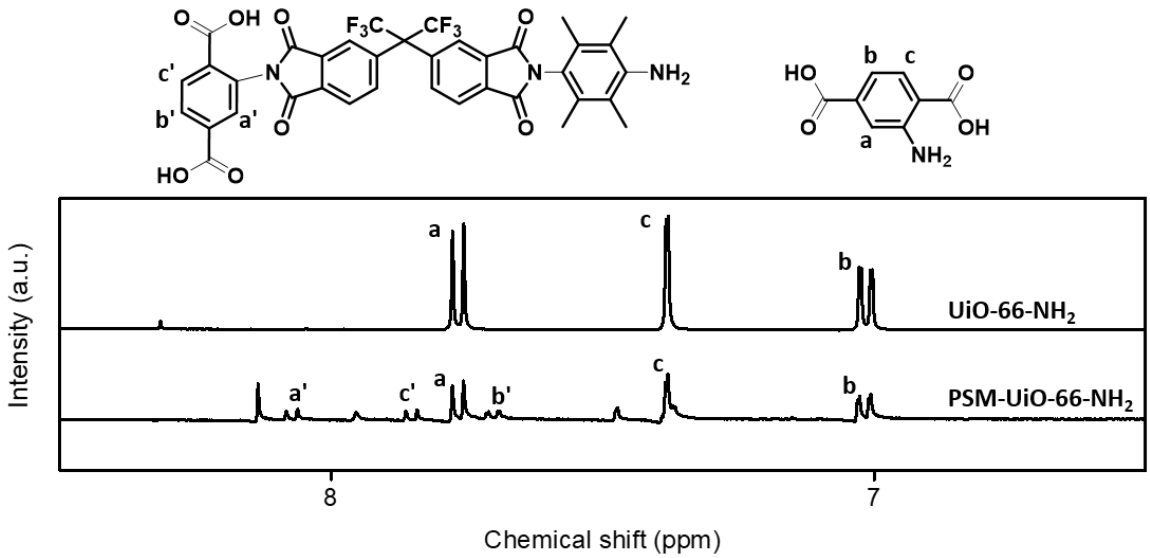

Figure S3. ^{1}H NMR spectra change upon 6FDA-Durene oligomer PSM of UiO-66-NH_2. Peaks were assigned according to the literature[10]. Unassigned peaks may result from coupling and exchange effects from HF and 6FDA-Durene oligomer.

Section B: Supporting characterization results for the MMMs and upper bound plots

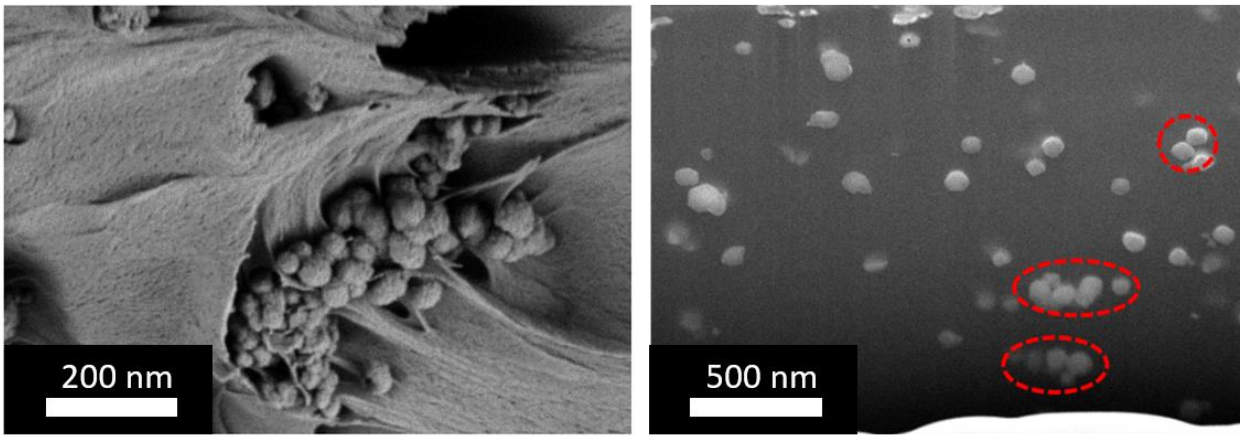

Figure S4. Cross-sectional FESEM (left) and FIB-SEM (right) images of 10% Pure MOF MMM. Both images show more serious particle aggregation than for the PSM-MOF MMMs.

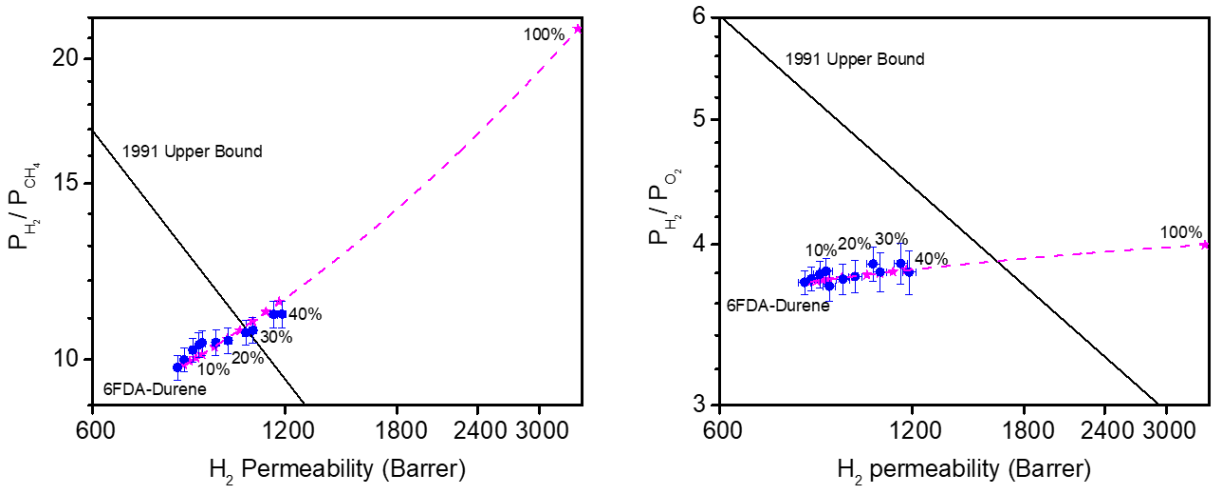

Figure S5. H_2/CH_4 and H_2/O_2 upper bound plots (blue circles: experimental data; pink stars: Maxwell Model predictions)

Table S1. CO_2/CH_4 separation data for MOF-based MMMs from the literature

MOF	Loading (wt%)	Polymer	Pressure (bar)	CO_2 permeability (Barrer)	Selectivity CO_2/CH_4	Ref.
6FDA-Durene/ UiO-66-NH_2	40	6FDA-Durene	1	1890	17.7	This work
NH_2-UiO-66-ABA	30	Matrimid®	9	37.9	47.7	Vankelecom, 2015[1]
UiO-66-NH_2	30	PAO-PIM-1	N.A.	8126	18.4	Jin, 2017[2]
UiO-66-NH_2	20	PIM-1 (in-situ crosslinking)	2	15815	19.1	Kaliaguine, 2018[3]
PEG@UiO-66-NH_2	40	PEBAX®	3	425	56	Qiao, 2017[4]

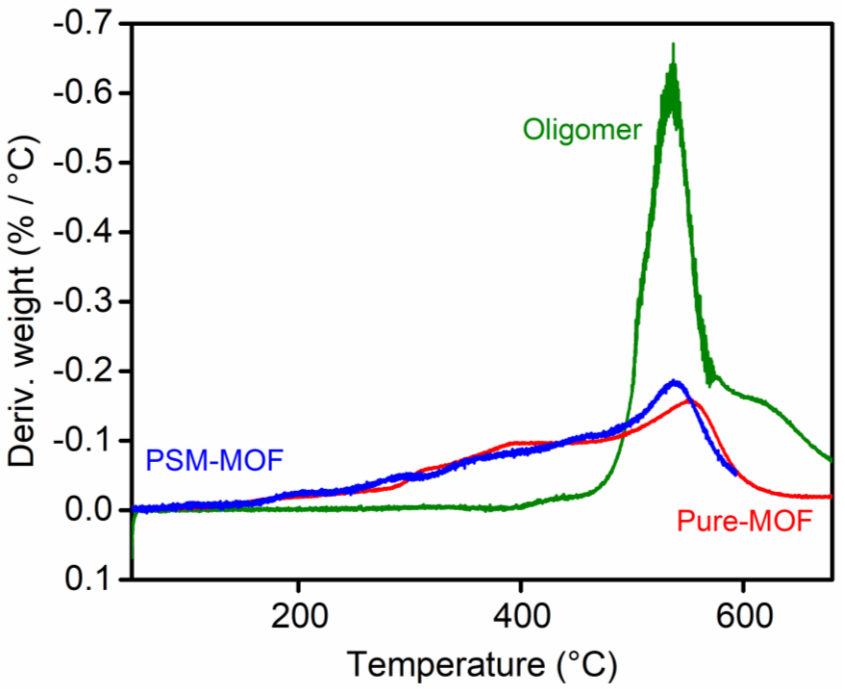

Figure S6. Derivative Thermal Gravimetric Analysis of the oligomer, Pure-MOF and PSM-MOF. Different stages of weight loss can be observed for the oligomer and the Pure-MOF.

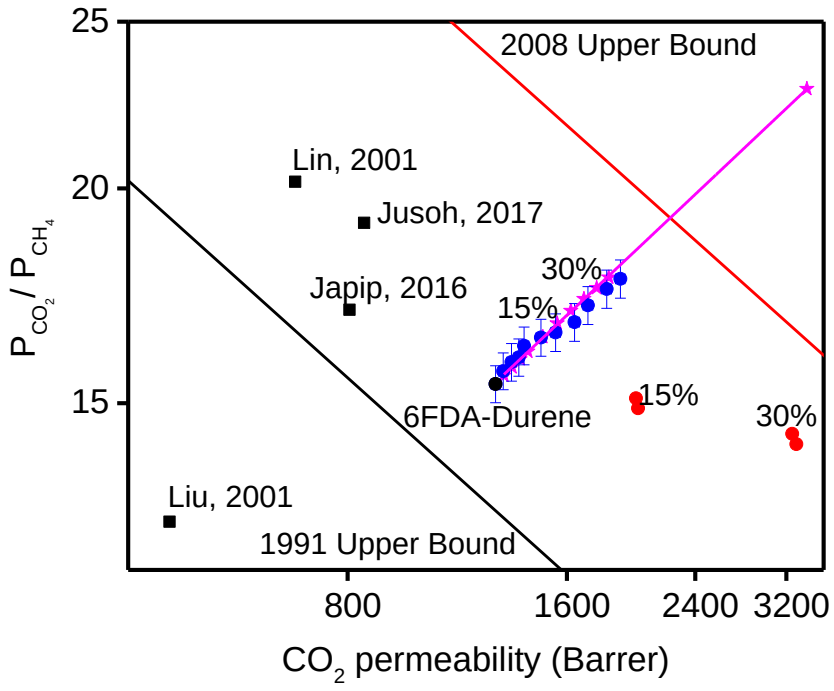

Figure S7. CO_2/CH_4 upper bound plot with comparative literature data for 6FDA-Durene (black circle: experimental data for 6FDA-Durene; blue circles: experimental data for PSM-MOF MMM; pink stars: Maxwell Model predictions; red circles: experimental data for Pure MOF MMM; black squares: literature data for 6FDA-Durene[6-9]). The difference in reported transport properties for 6FDA-Durene relates to differences in casting conditions and the temperature/pressure at which data were obtained.

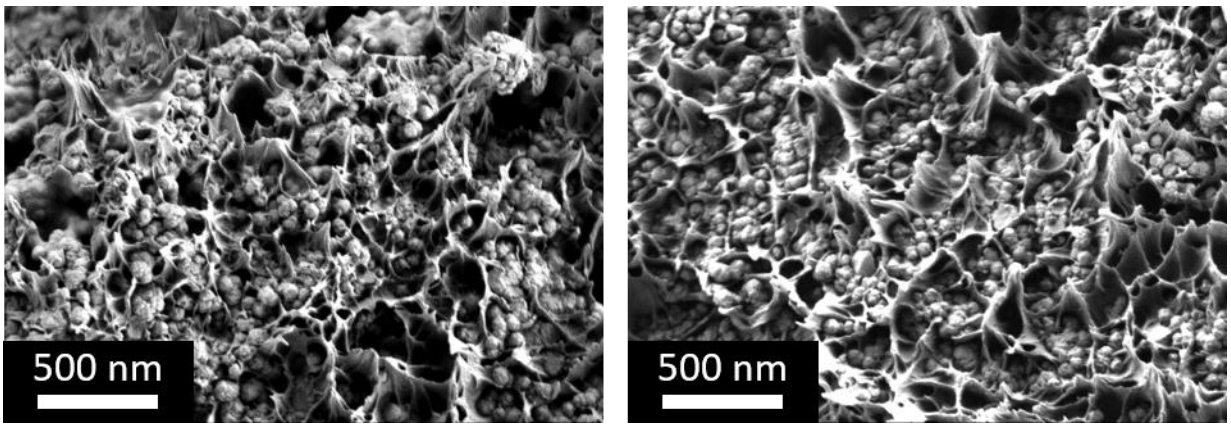

Figure S8. Cross-sectional SEM images of 40% PSM-MOF MMM taken near the top surface (left) and bottom surface (right).

Table S2. Permeation results for independently prepared samples of 6FDA-Durene and corresponding MMMs to evaluate reproducibility.

Loading (wt%)	Permeability (Barrer)									
	CH_4		N_2		O_2		H_2		CO_2	
	Trial 1	Trial 2	Trial 1	Trial 2	Trial 1	Trial 2	Trial 1	Trial 2	Trial 1	Trial 2
0%	83±3	81±3	86±3	85±3	218±7	210±7	820±20	810±20	1280±40	1250±40
2.5%	84±3	84±3	86±3	88±3	222±7	228±7	840±30	860±30	1310±40	1340±40
5%	84±3	86±3	86±3	87±3	227±7	232±7	860±30	870±30	1340±40	1360±40
7.5%	85±3	85±3	87±3	88±3	231±7	232±7	880±30	880±30	1370±40	1370±40
10%	86±3	88±3	87±3	89±3	240±7	250±7	890±30	890±30	1400±40	1410±40
15%	90±3	88±3	92±3	90±3	249±7	249±7	940±30	930±30	1470±40	1450±40
20%	94±3	92±3	97±3	95±3	259±8	254±8	980±30	960±30	1540±40	1510±40
25%	98±3	99±3	103±3	106±3	270±9	280±9	1040±30	1060±30	1640±50	1670±50
30%	100±3	104±3	106±3	109±3	281±9	288±9	1070±30	1090±30	1710±50	1760±50
35%	104±3	102±3	108±3	106±3	300±10	295±10	1150±40	1130±40	1810±60	1800±60
40%	107±3	106±3	109±3	107±3	310±10	308±10	1180±40	1160±40	1890±60	1870±60

Table S3. Permeation results for Pure MOF MMMs

Loading (wt%)	Permeability (Barrer)		Selectivity
	CH_4	CO_2	CO_2/CH_4
15%	132	1990	15.1
30%	226	3260	14.4

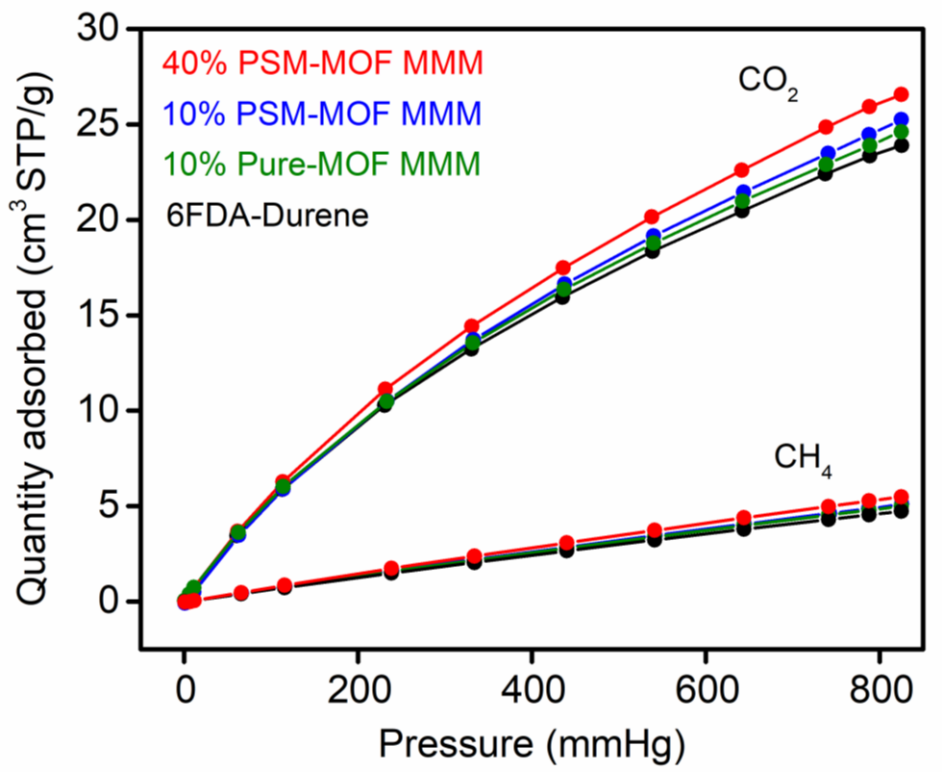

Figure S9. CO_2 and CH_4 sorption isotherms for 6FDA-Durene and corresponding MMMs.

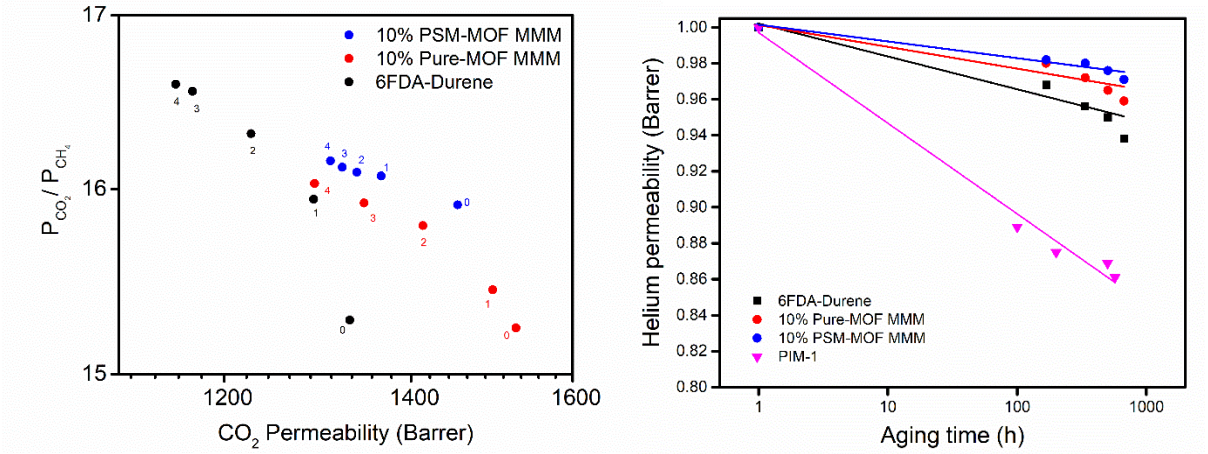

Figure S10. Physical aging of 6FDA-Durene and corresponding MMMs shown in CO_2/CH_4 upper bound plot (left) and normalized helium permeability plot (right). The number indicates the week number of a specific test. PIM-1 aging data was added as a reference.

Section C: Using the Maxwell model to predict transport in MMMs and volume fraction calculation

C1. Gas transport prediction using the Maxwell Model

Experimental data (P_{MMM}) at low loadings (below 20 wt%) were first used to calculate pure MOF permeability (P_f) for each gas. These values (P_{MMM} at loadings below 20 wt% and P_f) were then used together with the pure polymer permeability (P_p) to predict MMM permeabilities at all loadings. Volume fractions of MOF loading were calculated as described in section C2.

C2. Volume fraction calculation

TGA with an air sweep flow was used to determine the weight fraction of MOF fillers in MMMs. TGA profiles show that 6FDA-Durene decomposes completely under air flow at 700 °C (weight loss = 100%). Therefore, equation (1) was used to calculate the weight fraction of the MOF in the MMM:

$$MOF\ loading\ (wt\%) = \frac{wt\%\ remained\ of\ MMM\ at\ 700\ °C}{wt\%\ remained\ of\ pure\ MOF\ at\ 700\ °C} \quad (1)$$

To convert weight fraction to volume fraction, densities of the pure MOF and MMM are required. A crystal density of 1.36 g cm^{-3} for the pure UiO-66-NH_2 was taken from Mason *et al.*[5] Density of MMMs can be measured using a density kit attached to a Mettler Toledo mass balance (30029886). Equation (2) was then used to convert weight fraction to volume fraction:

$$MOF\ loading\ (vol\%) = \frac{MOF\ loading\ (wt\%)}{\rho_{MOF}}\rho_{MMM} \quad (2)$$

where, ρ_{MOF} and ρ_{MMM} are the densities of the MOF and MMM, respectively.

References

(1) Anjum, M. W.; Vermoortele, F.; Khan, A. L.; Bueken, B.; Vos, D. E. De; Vankelecom, I. F. J. Modulated UiO-66-Based Mixed-Matrix Membranes for CO_2 Separation. ACS Appl. Mater. Interfaces, 2015, 7, 25193–25201.

(2) Wang, Z.; Ren, H.; Zhang, S.; Zhang, F.; Jin, J. Polymers of Intrinsic Microporosity/Metal–organic Framework Hybrid Membranes with Improved Interfacial Interaction for High-Performance CO_2 Separation. J. Mater. Chem. A, 2017, 5, 10968–10977.

(3) Tien-Binh, N.; Rodrigue, D.; Kaliaguine, S. In-Situ Cross Interface Linking of PIM-1 Polymer and UiO-66-NH_2 for Outstanding Gas Separation and Physical Aging Control. J. Memb. Sci., 2018, 548, 429–438.

(4) Xie, K.; Fu, Q.; Kim, J.; Lu, H.; He, Y.; Zhao, Q.; Scofield, J.; Webley, P. A.; Qiao, G. G. Increasing Both Selectivity and Permeability of Mixed-Matrix Membranes: Sealing the External Surface of Porous MOF Nanoparticles. J. Memb. Sci., 2017, 535, 350–356.

(5) Mason, J. A.; Veenstra, M.; Long, J. R. Evaluating Metal-Organic Frameworks for Natural Gas Storage. Chem. Sci., 2014, 5, 32–51.

(6) Lin, W. H.; Chung, T. S. Gas Permeability, Diffusivity, Solubility, and Aging Characteristics of 6FDA-Durene Polyimide Membranes. J. Memb. Sci., 2001, 186, 183–193.

(7) Liu, S. L.; Wang, R.; Liu, Y.; Chng, M. L.; Chung, T. S. The Physical and Gas Permeation Properties of 6FDA-Durene/2,6-diaminotoluene Copolyimides. Polymer, 2001, 42, 8847-8855.

(8) Jusoh, N.; Yeong, Y. F.; Lau, K. K.; Shariff, A. M. Enhanced Gas Separation Performance Using Mixed Matrix Membranes Containing Zeolite T and 6FDA-Durene Polyimide. J. Memb. Sci., 2017, 525, 175-186.

(9) Japip, S.; Xiao, Y.; Chung, T. S. Particle-Size Effects on Gas Transport Properties of 6FDA-Durene/ZIF-71 Mixed Matrix Membranes. Ind. Eng. Chem. Res., 2016, 55, 9507–9517.

(10) Nagata, S.; Kokado, K.; Sada, K. Metal-Organic Framework Tethering PNIPAM for ON-OFF Controlled Release in Solution. Chem. Commum., 2015, 51, 8614-8617.